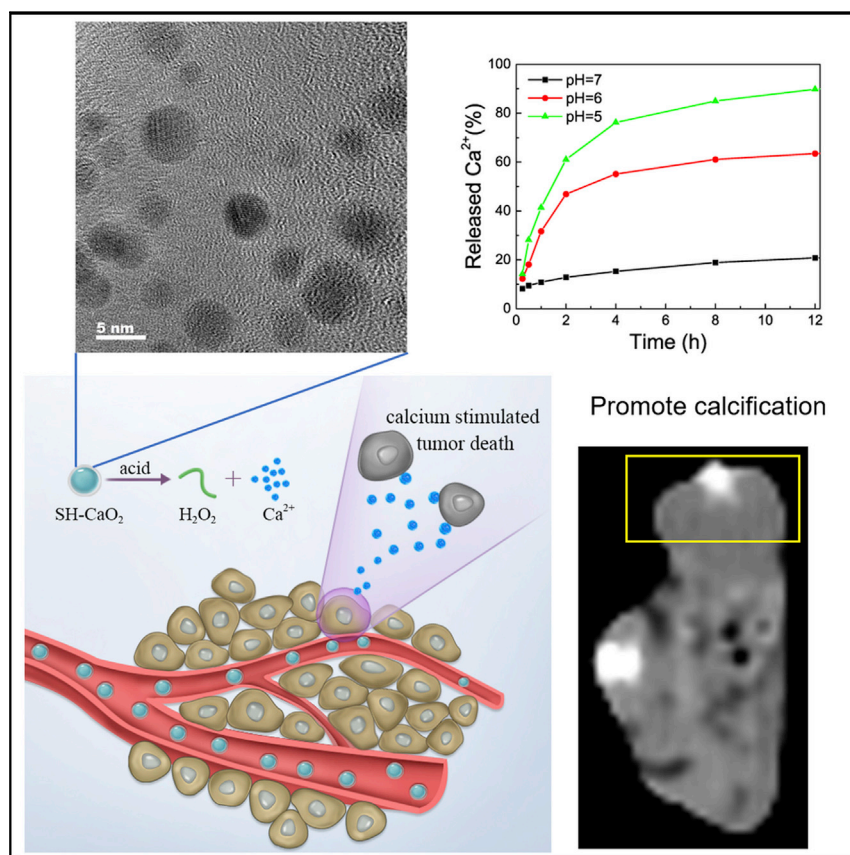


## Article

# Calcium-Overload-Mediated Tumor Therapy by Calcium Peroxide Nanoparticles



Meng Zhang, Ruixue Song, Yanyan Liu, ..., Yang Liu, Xiaogang Liu, Wenbo Bu

chmlx@nus.edu.sg (X.L.)  
wbbu@chem.ecnu.edu.cn (W.B.)

### HIGHLIGHTS

A simple synthetic strategy for ultrasmall calcium peroxide nanoparticles is reported

The nanoparticles show pH-sensitive calcium ions and H<sub>2</sub>O<sub>2</sub> release

The release behavior realizes tumor calcium overload and promotes calcification

Great antitumor efficacy is verified for modified calcium peroxide nanoparticles

With their unique biological effects on tumor microenvironment, catabolites of nanoparticles can make a significant difference for tumor suppression. We report a facile synthesis method of ultrasmall calcium peroxide nanoparticles and demonstrate their rapid decomposition in tumor region. This can trigger a destructive calcium overload process in tumor cells, lead to cell death, and further tissue calcification, which also allows for medical imaging.

Article

# Calcium-Overload-Mediated Tumor Therapy by Calcium Peroxide Nanoparticles

Meng Zhang,<sup>1,2</sup> Ruixue Song,<sup>3</sup> Yanyan Liu,<sup>3</sup> Zhigao Yi,<sup>4</sup> Xianfu Meng,<sup>3</sup> Jiawen Zhang,<sup>5</sup> Zhongmin Tang,<sup>1,2</sup> Zhenwei Yao,<sup>5</sup> Yang Liu,<sup>3</sup> Xiaogang Liu,<sup>4,\*</sup> and Wenbo Bu<sup>1,3,6,\*</sup>

## SUMMARY

Calcium overload, characterized by an abnormal cytoplasm accumulation of free calcium ions ( $\text{Ca}^{2+}$ ), is a widely recognized cause of damage in numerous cell types and even of cell death. This undesirable destructive process can become a new tool applicable to cancer treatment. Herein, on the basis of the unique biological effect of  $\text{Ca}^{2+}$ , we demonstrate a highly efficient strategy for tumor therapy by utilizing pH-sensitive sodium-hyaluronate-modified calcium peroxide nanoparticles (SH- $\text{CaO}_2$  NPs). These NPs create an artificial calcium overloading stress in tumor cells, which is responsible for cell death. Notably, the killing effect is not limited to tumor types or hypoxic cells, and normal cells are more tolerant of the adverse influence of NPs than tumor cells. The  $\text{Ca}^{2+}$  enrichment also increases the likelihood of tumor calcification, which could contribute to *in vivo* tumor inhibition and facilitate medical imaging to monitor the treatment efficacy.

## INTRODUCTION

In clinical tumor treatment, internal calcification has frequently been observed after radiotherapy or chemotherapy in certain tumor types.<sup>1–3</sup> Calcification may be associated with tumor cell death, but the intrinsic cause of cell death remains unknown. It is well known that the common biological effect of chemotherapy drugs and high-energy radiation is the production of a large number of free radicals in tumor cells.<sup>4–6</sup> Calcification, a slow progression of calcium salt deposition in local tissues initiated by the accumulation of localized calcium ions, is a possible outcome of the calcium overload process.<sup>7–9</sup> These factors suggest that the process of calcification comprises a series of secondary reactions caused by free-radical-induced intracellular calcium overload. However, this possibility cannot fully explain why tumors that have become calcified over time often show better treatment response.

Given the importance of calcium ions in multiple cellular processes, including proliferation, metabolism, and death,<sup>10</sup> there may be an alternative explanation. While free radicals exert strong anticancer effects mainly by directly attacking double-stranded DNA sequences and causing irreparable proliferation-related damage, free-radical-induced calcium signaling disorders are also considered to contribute to cell death. In other words, the induced calcium overloading process is not an inconsequential or trivial process but could be another efficient “destructive factor” against tumor cells in addition to free radicals. Likewise, calcification is not a mere by-product of cancer treatment but a strong proof and external manifestation of the role of the calcium overload mechanism. Overall, free radicals and calcium overload in cells do not merely share mutual causation but a mutual reinforcement or synergistic effect for tumor therapy. Unfortunately, the cell-damaging functions of  $\text{Ca}^{2+}$

## The Bigger Picture

Metal ions with diverse cellular biological effects can play more important roles in cell metabolism and proliferation than expected. Any alteration of the metal-content balance could induce a series of intracellular responses, even cell death. Ferroptosis is one of the typical examples that have been applied in tumor treatment. This inspires further studies of other functional metal ions and the development of novel strategies for efficient cancer therapy. We report the design of pH-responsive calcium peroxide nanoparticles and show that the quick release of calcium ions under tumor microenvironment can efficiently induce calcium overload and calcification, which are both damaging against tumor survival. *In vivo* evaluation also reveals the tumor-suppression efficiency by modified nanoparticles. This strategy, which is denoted as ion-interference therapy, highlights the availability of other metal ions in oncology and opens a new door for further clinical cancer treatment.

have been long neglected in designing nanomaterial-based antitumor drugs, and there are almost no reports on the development of calcium-based nanomedicine to induce intracellular calcium overloading for combined treatment.

Herein, by making good use of the unique cytotoxicity mechanism of  $\text{Ca}^{2+}$ , we prepared calcium peroxide nanoparticles ( $\text{CaO}_2$  NPs) to demonstrate the unexplored role of calcium overload in tumor therapy, which is of equal importance to reactive oxygen species (ROS), and further elaborated its great potential in clinical cancer treatment.  $\text{CaO}_2$  NPs are pH sensitive and would slowly decompose into free  $\text{Ca}^{2+}$  and  $\text{H}_2\text{O}_2$  in the acidic tumoral microenvironment,<sup>11,12</sup> leading to intracellular calcium overload and oxidative stress, respectively, in cells at the same time. For tumor cells in which catalase (CAT) is downregulated,<sup>13</sup> the constant challenge from oxidative stress would alter protein functions, resulting in the desensitization of calcium-related channels followed by an uncontrollable cellular accumulation of  $\text{Ca}^{2+}$ .<sup>14</sup> This biological effect could hinder the accurate transmission of calcium signals and induce cell death.<sup>10,15</sup> Meanwhile, the enrichment of  $\text{Ca}^{2+}$  is more likely to engender tumor calcification, which would benefit *in vivo* tumor inhibition and simultaneously facilitate computed tomography (CT) imaging diagnosis of the treatment efficacy.<sup>31,32</sup> By comparison, healthy cells are more tolerant of the adverse influence of NPs. This could be attributed to the presence of a sufficient amount of CATs that prevent oxidative activation of the cells and thus allow the exogenous  $\text{Ca}^{2+}$  to be more efficiently pumped out or stored through calcium channels (Figure 1). When stabilized with sodium hyaluronate through surface modification, these  $\text{CaO}_2$  NPs are stable in body fluids until the protective layer is degraded by hyaluronidase.<sup>16,17</sup> Considering the negligible systemic biological toxicity of  $\text{Ca}^{2+}$ , ease of particle synthesis, and economically available raw materials, we believe that sodium-hyaluronate-modified calcium peroxide nanoparticles (SH- $\text{CaO}_2$  NPs) have potential utilities for clinical applications in cancer therapy. Besides, the strategy of ion-interference tumor therapy may also hold promise as an effective cancer therapeutic tool complementary to traditional clinical tumor treatment.

## RESULTS

### Characterization of SH- $\text{CaO}_2$ NPs

Sodium-hyaluronate-modified  $\text{CaO}_2$  NPs were prepared through a simple and quick wet-chemistry method in a methanol-water system at room temperature. As shown in transmission electron microscopy (TEM) images, the obtained NPs had good crystallinity, with an average particle size smaller than 5 nm (Figures 2A and 2B), which could be regulated by changing the alkalinity of the mixture during preparation. X-ray diffraction (XRD) characterization confirmed that the diffraction peaks of the as-prepared products are well in accord with those of the tetragonal  $\text{CaO}_2$  standard card (PDF#03-0865), signifying the successful formation of  $\text{CaO}_2$  crystalline NPs (Figure 2C). Effective modification with sodium hyaluronate, which was performed alongside the nucleation and growth of the  $\text{CaO}_2$  NPs to confine the grain size, was achieved by the attraction between the negatively charged ions and positively charged nanocrystals.<sup>18</sup> The zeta-potential changes of the NPs verified this supposition, as the zeta potential decreased by approximately 10 mV after the modification (Figure S1), and thermogravimetric analysis (TGA) showed a greater mass loss, which further indicated the efficient modification (Figure S2). In addition, while the hydrodynamic size distribution was narrow, the hydrodynamic diameter seemed to be larger than the one displayed in the TEM images (Figure S3). This discrepancy could be partially explained by the hydrogen bonding networks among the NPs, which is consistent with the appearance of a broad absorption peak at 3,600–3,200  $\text{cm}^{-1}$  in the Fourier transform infrared (FTIR) absorption spectrum that

<sup>1</sup>State Key Laboratory of High Performance Ceramics and Superfine Microstructures, Shanghai Institute of Ceramics, Chinese Academy of Sciences, Shanghai 200050, China

<sup>2</sup>University of Chinese Academy of Sciences, Beijing 100049, China

<sup>3</sup>Shanghai Key Laboratory of Green Chemistry and Chemical Processes, School of Chemistry and Molecular Engineering, East China Normal University, Shanghai 200062, China

<sup>4</sup>Department of Chemistry, National University of Singapore, Singapore 117543, Singapore

<sup>5</sup>Department of Radiology, Huashan Hospital, Fudan University, Shanghai 200040, China

<sup>6</sup>Lead Contact

\*Correspondence: [chmlx@nus.edu.sg](mailto:chmlx@nus.edu.sg) (X.L.), [wbbu@chem.ecnu.edu.cn](mailto:wbbu@chem.ecnu.edu.cn) (W.B.)

<https://doi.org/10.1016/j.chempr.2019.06.003>

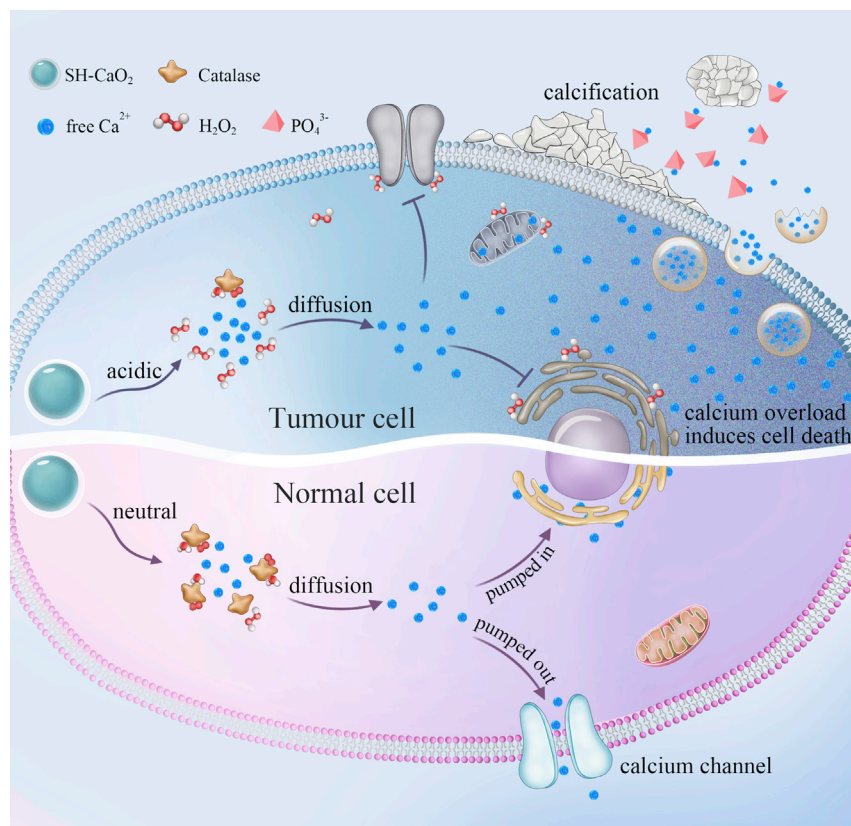


**Figure 1. Schematic Representation of the Functional Pattern of SH-CaO<sub>2</sub> NPs**

In the acidic microenvironment of a tumor region, SH-CaO<sub>2</sub> NPs are decomposed into Ca<sup>2+</sup> and H<sub>2</sub>O<sub>2</sub> molecules. The low expression of catalase in tumor cells causes abnormal cellular H<sub>2</sub>O<sub>2</sub> accumulation and an imbalanced calcium transport pathway, thereby resulting in an efficient cellular calcium overload and subsequently the induction of cell death. Meanwhile, the enriched local concentration of Ca<sup>2+</sup> increases the likelihood of tumor calcification.

represents the hydrogen-bonded O–H stretching vibration (Figure S4). Moreover, the characteristic peaks around 831, 881, and 1,115 cm<sup>-1</sup> also verified the existence of peroxide groups.<sup>19</sup>

The pH-triggered release of Ca<sup>2+</sup> by the decomposition of CaO<sub>2</sub> NPs was then evaluated in various pH buffers. Within 12 h, fewer than 10% of the Ca<sup>2+</sup> were released at pH 7.0, whereas more Ca<sup>2+</sup> was produced in a mimetic acidic microenvironment, with approximately 50% discharge at pH 6.0 and 80% at pH 5.0 (Figure 2D). This suggested that the CaO<sub>2</sub> NPs were pH sensitive and would decompose into Ca<sup>2+</sup> in an acidic microenvironment. The reason was unambiguous: in contrast to the slow progression of hydrolysis relying on protons produced by water ionization under neutral conditions, the decomposition speed of CaO<sub>2</sub> NPs would be suddenly accelerated in an acidic environment, depending on the proton concentrations surrounding the NPs. The chemical reaction equation could be written as follows:



Unlike Ca<sup>2+</sup> already existing in the blood, the leakage of oxidizing H<sub>2</sub>O<sub>2</sub> in the blood is not favored. Therefore, sodium hyaluronate as a protective layer was modified on the surface of CaO<sub>2</sub> NPs. The layer could block the direct exposure of the CaO<sub>2</sub> core

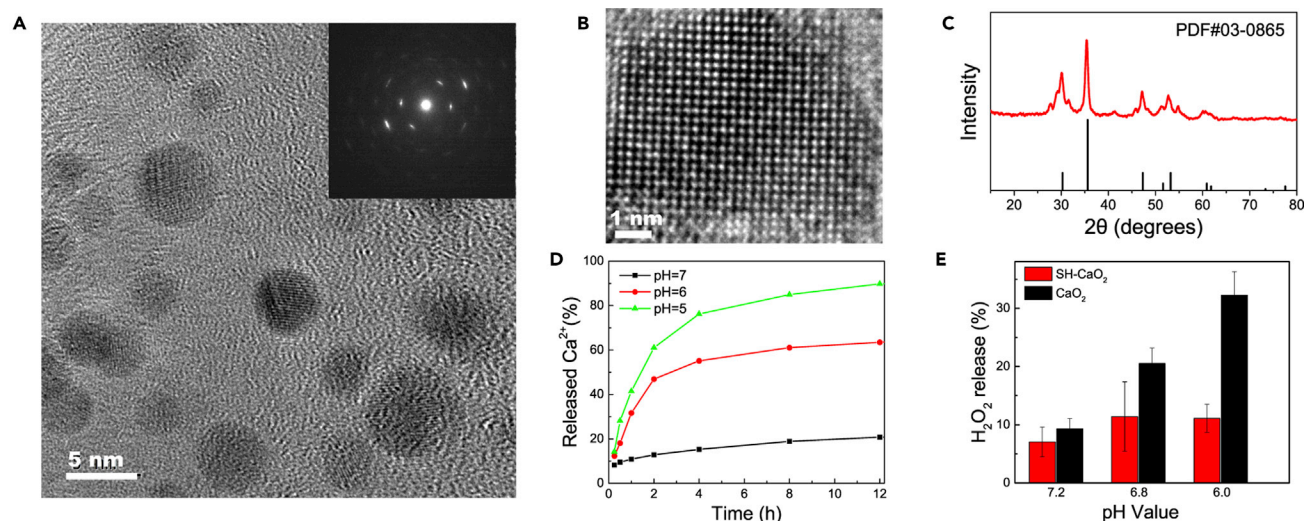


**Figure 2. Characterization of SH-CaO<sub>2</sub> NPs**

(A) TEM images of calcium peroxide nanoparticles (inset: a TEM electron diffraction image).

(B) High-resolution TEM image of the calcium peroxide nanocrystals.

(C) X-ray powder diffraction pattern of the SH-CaO<sub>2</sub> NPs.

(D) Time-dependent Ca<sup>2+</sup> release from the CaO<sub>2</sub> NPs dispersed in buffer solutions of different pH values. The release of calcium was clearly accelerated under acidic conditions.

(E) H<sub>2</sub>O<sub>2</sub> production via CaO<sub>2</sub> and SH-CaO<sub>2</sub> NPs over a 2 h timespan at different pH values. The decomposition of NPs was prevented after surface modification with sodium hyaluronate.

Data are represented as mean ± SD.

to the surrounding protons, thus reducing the degradation of SH-CaO<sub>2</sub> NPs during blood circulation (pH 7.4). Moreover, the -COO<sup>-</sup> groups in the sodium hyaluronate molecule tended to compete for protons and bind them, which further increased the resistance to some weak pH oscillations. In comparison with unmodified NPs, SH-CaO<sub>2</sub> NPs generated less H<sub>2</sub>O<sub>2</sub> under slightly acidic buffer solution, implying that the modified NPs were less harmful before arrival in the tumor region (Figures 2E and S5). Upon uptake by tumor cells, the protective sodium hyaluronate layer of the NPs could be degraded by intracellular hyaluronidase and the CaO<sub>2</sub> core begins to take the therapeutic effect.

### In Vitro Cytotoxicity Mechanism of SH-CaO<sub>2</sub> NPs

As a second messenger in intracellular signal transmission, calcium signals are sent through the activation or inactivation of specific targets (proteins, nucleic acids, etc.) to control vital physiological processes, which is achieved essentially under the fluctuations in local calcium concentration.<sup>20,21</sup> Any Ca<sup>2+</sup> concentration changes caused by non-cellular regulation would disturb the calcium signals and influence multiple cell activities. In particular, under oxidative stress, the calcium channels in a cell are functioning abnormally, and the cellular Ca<sup>2+</sup> concentration becomes difficult to re-modulated to a normal state, resulting in calcium-overload-induced cell death.<sup>14</sup> This process can be defined as “calcicoptosis.” The hypothesis was firstly evidenced by a simple treatment of Ca<sup>2+</sup> plus H<sub>2</sub>O<sub>2</sub> with 4T1 cells, which showed a sharp decrease in cell viability and an enhancement of intracellular Ca<sup>2+</sup> concentration (Figure S6). Then, SH-CaO<sub>2</sub> NPs were studied in detail. While incubation with Ca<sup>2+</sup> alone or a low concentration of pH-sensitive SH-CaO<sub>2</sub> NPs was harmless to 4T1 cells, higher concentrations of NPs demonstrated a rapid increase in cytotoxicity (Figure 3A). This result could be explained by the excessive hydrogen-peroxide-induced oxidative stress, switching the regulatory “Ca<sup>2+</sup> code” to a signal for cell

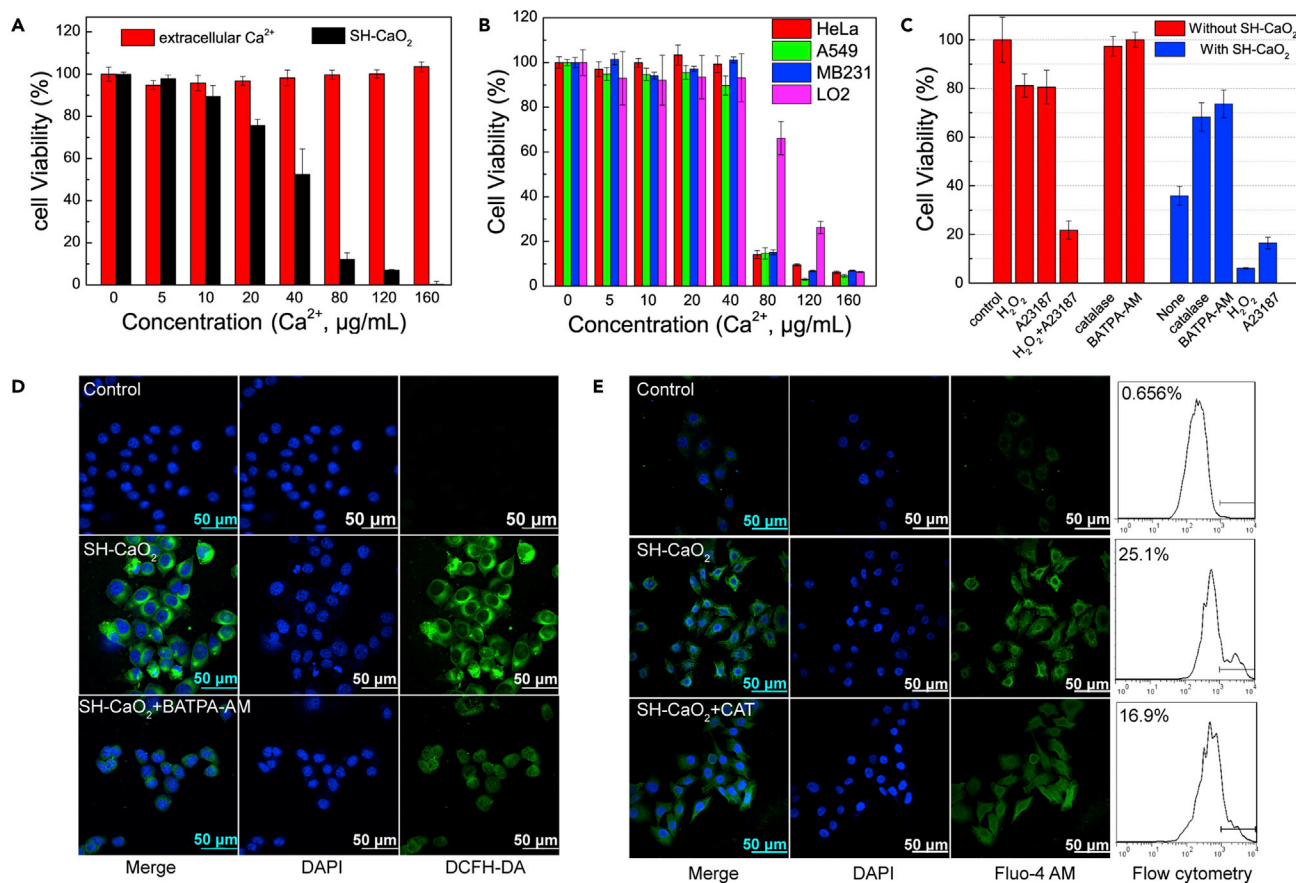


**Figure 3. SH-CaO<sub>2</sub> NPs Could Efficiently Induce Tumor Cell Death by Releasing Massive Amounts of Free Calcium and H<sub>2</sub>O<sub>2</sub>**

(A) Cell-viability assay in 4T1 cells incubated with CaCl<sub>2</sub> or SH-CaO<sub>2</sub> NPs.

(B) Cell-viability assay in human tumor cells (HeLa, A549, and MB231) or normal cells (LO2) incubated with SH-CaO<sub>2</sub> NPs. Normal cells were more tolerant of SH-CaO<sub>2</sub> NPs.

(C) Cell-viability assay in 4T1 cells incubated with or without SH-CaO<sub>2</sub> NPs and different reagents, including A23187 (calcium ionophores), BAPTA-AM (calcium chelators), H<sub>2</sub>O<sub>2</sub>, and catalase. Ca<sup>2+</sup> played an essential role in cell death and were of equal importance to H<sub>2</sub>O<sub>2</sub>.

(D) ROS production in 4T1 cells after SH-CaO<sub>2</sub> NP treatment.

(E) Free-calcium generation in 4T1 cells after SH-CaO<sub>2</sub> NP treatment.

Data are represented as mean ± SD.

death. Satisfactorily, the remarkable killing effect was not limited by tumor type, as the SH-CaO<sub>2</sub> NPs could efficiently destroy multiple types of human tumor cells, including cervical, breast, and lung carcinoma, whereas normal human cells managed to tolerate the adverse influence of NPs with much higher cell viabilities than tumor cells under the same treatment. This higher tolerance was attributed to the presence of a sufficient amount of CAT to prevent the normal cells from entering an oxidative stress state caused by excessive H<sub>2</sub>O<sub>2</sub> (Figure 3B). Furthermore, SH-CaO<sub>2</sub> NPs were still effective against hypoxic tumor cells, with approximately 80% cell damage when incubated with 1 mmol/L NPs, revealing the potential of treating hypoxic tumors (Figure S7).

To further validate the pivotal role of calcium overload in cell death, we first incubated H<sub>2</sub>O<sub>2</sub> and A23187, a calcium ionophore that specifically carries extracellular Ca<sup>2+</sup> into cells, concurrently with 4T1 cells for 24 h, simulating the working pattern of SH-CaO<sub>2</sub> NPs in cells. In contrast to the 80% cell viabilities after treatment with H<sub>2</sub>O<sub>2</sub> or A23187 alone, the cell survival rate of “simulated NPs” dropped sharply

to approximately 22% at the same concentration. Moreover, when the excessive  $\text{Ca}^{2+}$  ions (or  $\text{H}_2\text{O}_2$ ) released by SH- $\text{CaO}_2$  NPs were inhibited by the calcium chelator BAPTA-AM (or CAT), the NP-induced cell damage was reduced by more than half; in contrast, the addition of extra calcium ionophores (or  $\text{H}_2\text{O}_2$ ) along with SH- $\text{CaO}_2$  NPs would double the cell death (Figure 3C). All these results illustrated that the role of  $\text{Ca}^{2+}$  was as important as that of  $\text{H}_2\text{O}_2$  in the  $\text{CaO}_2$ -induced cell death procedure *in vitro*.

The generation of ROS and  $\text{Ca}^{2+}$  was then monitored by confocal laser scanning microscopy (CLSM). The control group exhibited weak green luminescence, while the group cultivated with SH- $\text{CaO}_2$  NPs exhibited strong intracellular luminescence, indicating the release of the exogenous free  $\text{Ca}^{2+}$  and  $\text{H}_2\text{O}_2$  (Figures 3D and 3E). Interestingly, the addition of calcium chelators decreased the  $\text{H}_2\text{O}_2$  output, as the fluorescence weakened after treatment with NPs and BAPTA-AM. Similarly, the intracellular free- $\text{Ca}^{2+}$  output was also reduced by incubation with CAT and NPs (Figure 3E). This phenomenon further indicates the interrelationship between calcium and  $\text{H}_2\text{O}_2$  in cells.<sup>20–23</sup> Because both are signaling molecules, the induced increases of calcium overload and ROS will create a self-amplifying loop in cells.<sup>22,23</sup> On the one hand, the cytosol  $\text{Ca}^{2+}$  accumulation will stimulate NADPH oxidase activity that is responsible for ROS generation, and the process of  $\text{Ca}^{2+}$ -promoted ATP synthesis can also induce the respiratory chain electron leakage and ROS levels increase.<sup>24</sup> On the other hand, ROS increase can provoke  $\text{Ca}^{2+}$  entry by modulating the plasma membrane  $\text{Ca}^{2+}$  channels (e.g., VDCC, TRP, and SOCE), intracellular calcium channels (e.g., RyR and  $\text{IP}_3\text{R}$ ), and  $\text{Ca}^{2+}$ ATPases. Therefore, although the incubated SH- $\text{CaO}_2$  NPs can release  $\text{Ca}^{2+}$  and  $\text{H}_2\text{O}_2$ , the detected calcium and ROS fluorescence signal is not just for the SH- $\text{CaO}_2$  NPs degradation but also involves the result of cellular stress responses. Downregulating calcium levels (or ROS levels) can relieve the cellular stress response, and cells can jump out of the self-amplifying loop with self-regulation to a chemical equilibrium. As a result, the collected ROS (or calcium) signals finally decreased.

To further “visualize” the intracellular degradation of SH- $\text{CaO}_2$  NPs, we cultivated cells loaded with fluorescent probes with NPs for 4 h and imaged them every 80 s by CLSM (Video S1). In the first 22 min, in addition to the “calcium sparks” phenomenon,<sup>25,26</sup> we observed dynamic increases in green and red fluorescence, which was direct proof of the generation of  $\text{Ca}^{2+}$  and  $\text{H}_2\text{O}_2$  in the cells (Figures 4A, 4B, and S8). Unexpectedly, the intracellular release of  $\text{Ca}^{2+}$  coincided with an exocytosis process of excessive calcium, accompanied by the formation of numerous small vesicles outside the cell membrane (Videos S2 and S3). Meanwhile, after incubation with SH- $\text{CaO}_2$  NPs, the cell nucleus became condensed, and the mitochondrial activity was drastically reduced (Figures 4C and S9);<sup>27</sup> there were further distinguishing morphological changes of apoptosis in the microstructure, such as the marginalization and densification of chromatin into dense masses, mitochondrial swelling, and the vesicular-like expansion and vacuolization of the endoplasmic reticulum (Figure 4D).<sup>28</sup> All these phenomena further indicate that the calcium overload had seriously disturbed the normal proliferation of cells and ultimately resulted in cell death.

#### Formation of Calcified Nodules by SH- $\text{CaO}_2$ NPs

Accompanied by the cell uptake of SH- $\text{CaO}_2$  NPs, we also observed the formation of small vesicles outside of the cell membrane, which was a very fast process that spanned only a few minutes (Figure 5A). Since the formed small vesicles contained high concentrations of free  $\text{Ca}^{2+}$  similar to those in matrix vesicles (MVs; extracellular organelles formed by chondrocytes or bone cells that functions in osteogenesis and

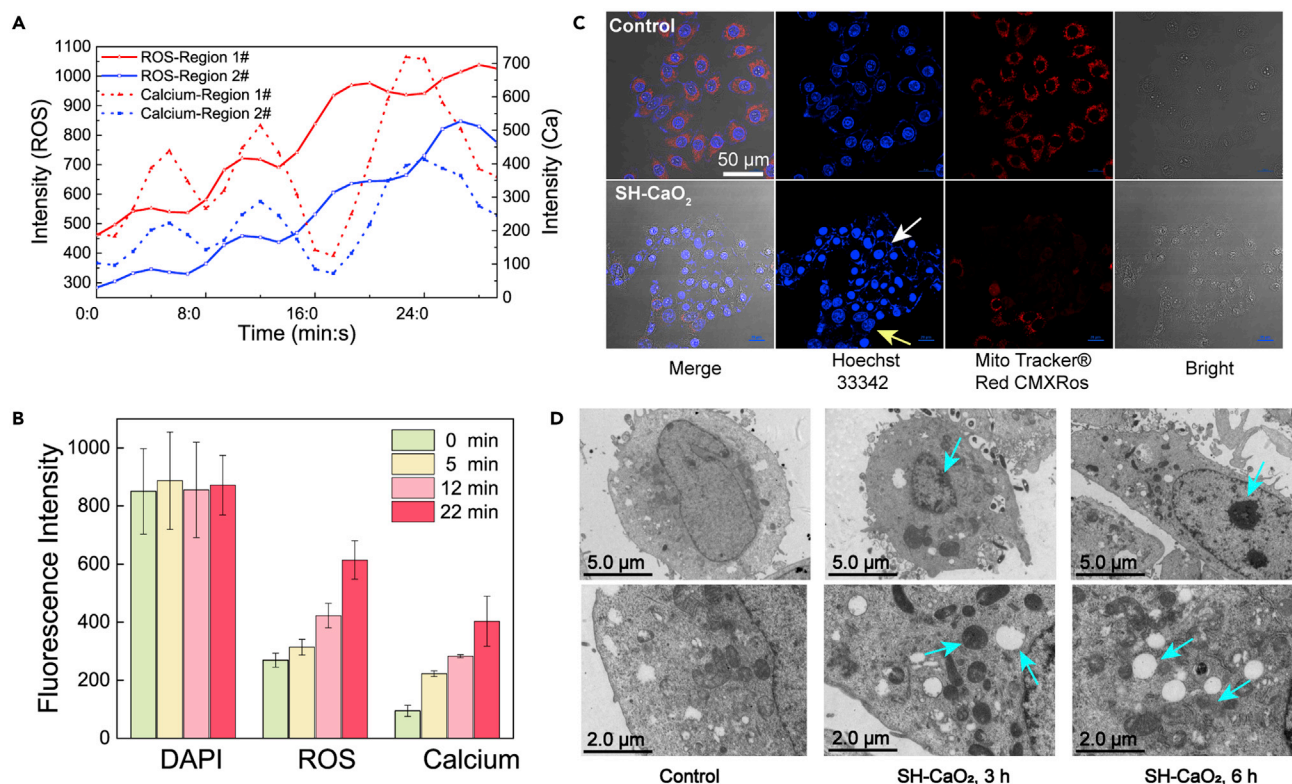


**Figure 4. Visualization of the Cellular Release of H<sub>2</sub>O<sub>2</sub> and Ca<sup>2+</sup> and of Cell Death**

(A) Time-dependent fluorescence intensity of ROS and calcium in different regions of interest (ROIs) by CLSM (see also Figure S8 and Video S1).

(B) Average fluorescence-intensity changes of ROS and calcium in the marked ROI show intracellular degradation of SH-CaO<sub>2</sub> NPs. Data are represented as mean ± SD.

(C) Changes of the nucleus and mitochondrial membrane potential before and after the SH-CaO<sub>2</sub> NP treatment as observed by CLSM. The yellow arrow indicates a normal nucleus, whereas the white arrow indicates a condensed nucleus.

(D) Morphological changes in subcellular organelles of tumor cells before and after treatment with SH-CaO<sub>2</sub> NPs for 3 or 6 h (observed by bio-TEM) confirm that the SH-CaO<sub>2</sub>-NP-induced calcium overload resulted in tumor death.

mineralization),<sup>29,30</sup> they were considered to have the same self-calcification ability. Indeed, energy dispersive X-ray (EDX) analysis confirmed the existence of O, Ca, and P elements within the vesicles (Figures 5C, 5D, and S10). Additionally, the collections of cells undergoing exocytosis were also characterized to be the hydroxyapatite phase by XRD, which further validated the calcification potential of the MV-like vesicles (Figure 5B). Biom mineralization was then performed *in vitro* and measured by Alizarin Bordeaux and von Kossa staining, two staining methods that are frequently applied to detect calcified nodules, which are dyed red and black, respectively. In contrast with the control group, there was a wide calcified area in the group incubated with SH-CaO<sub>2</sub> NPs for 6 h; after 12 h of treatment, almost all cells were thoroughly mineralized (Figure 5E). Moreover, this biom mineralization could remain in place *in vivo* and be imaged by a CT scanner. In the tumor-bearing mouse model, despite the weakly enhanced CT signal 3 h after the injection, SH-CaO<sub>2</sub> NPs could speed up the process of tumor calcification. Three days after a single injection, the tumor region was reduced and brightened in the CT image; for the larger tumor model, the densified microcalcification was more apparent after multiple injections (Figures 6A and 6B). Histological analysis of the tumor sections further illustrated the existence of tumor calcification (Figures 6C and S11). This satisfactory calcification effect would benefit the *in vivo* tumor inhibition and facilitate CT imaging to monitor the efficacy of treatment as well.<sup>31,32</sup>

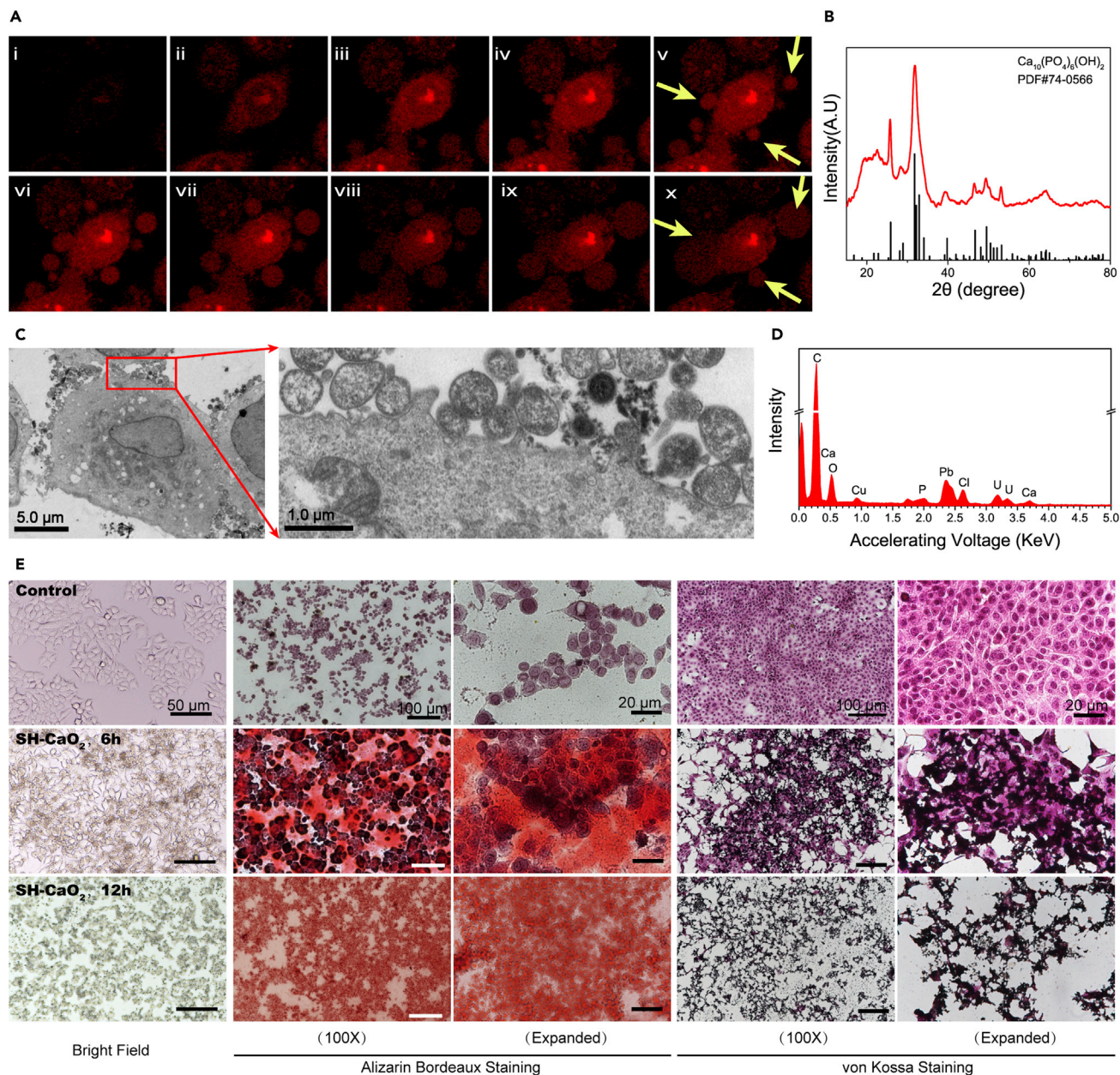


**Figure 5. The Observation and Identification of Cell Calcification *In Vitro***

(A) The formation and exocytosis of calcium-enriched small vesicles after treatment with SH-CaO<sub>2</sub> NPs, as shown in a single cell (yellow arrows). The intracellular free-calcium ions were tracked by a calcium red fluorescent probe (see also [Videos S2 and S3](#)).

(B) X-ray powder diffraction pattern of the collected products from cell exocytosis after treatment with SH-CaO<sub>2</sub> NPs.

(C) Bio-TEM images of 4T1 cells after treatment with SH-CaO<sub>2</sub> NPs for 6 h show the formation of small vesicles outside of the membrane (see also [Figure S10](#)).

(D) Energy-dispersive X-ray (EDX) spectrum of the products of exocytosis after the treatment of SH-CaO<sub>2</sub> NPs shows the existence of mineralization. Cell samples were stained with uranium salts and lead salts for TEM observation.

(E) Identification of the products of exocytosis *in vitro* with Alizarin Bordeaux staining and von Kossa staining, which show the calcified areas in red and black, respectively.

### ***In Vivo* Tumor Growth Inhibition by SH-CaO<sub>2</sub> NPs**

The antitumor therapeutic effect of SH-CaO<sub>2</sub> NPs was next evaluated in a 4T1 subcutaneous tumor model and an orthotopic tumor model *in vivo*. First, the SH-CaO<sub>2</sub> NPs were proved to be biocompatible and tolerated under the dosage of 75 mg/kg

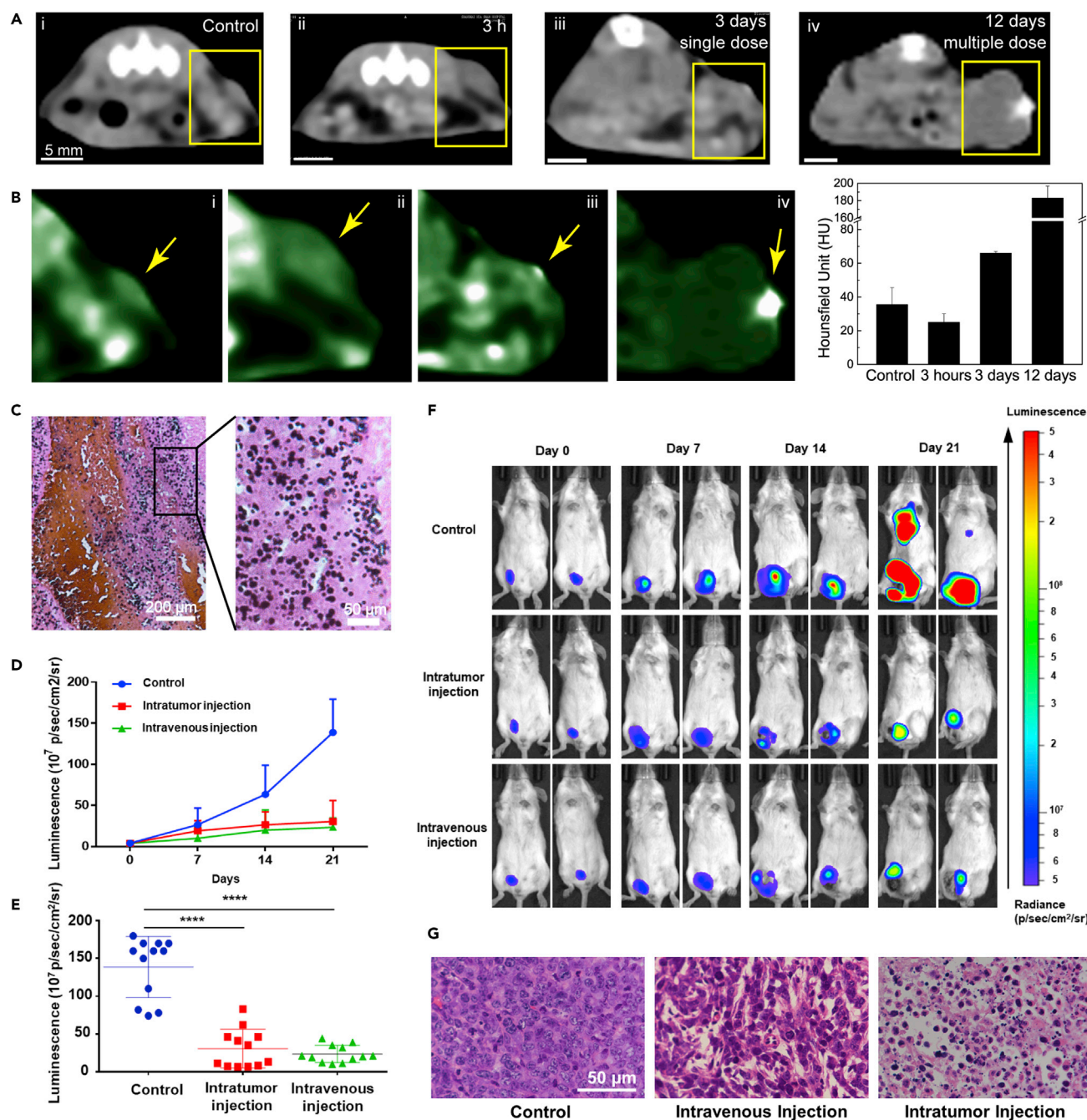


**Figure 6. Identification of Calcification in the Tumor Region and Tumor-Growth Inhibition In Vivo**

(A) CT images of mice after the following treatments: (i) control, (ii) 3 h after the intratumor injection of SH-CaO<sub>2</sub> NPs, (iii) 3 days after the injection of a single dose of SH-CaO<sub>2</sub> NPs for a small tumor, and (iv) 12 days after the injection of multiple dose (four times, injected every 2 days) for a larger tumor.

(B) Pseudocolor CT images of tumors (i–iv) and the corresponding Hounsfield unit (HU) values of the microcalcification.

(C) von Kossa staining of tumor tissue sections after multiple injections with SH-CaO<sub>2</sub> NPs.

(D) Tumor luminescence changes of different groups after varied treatments (n = 12 in each group).

(E) Tumor luminescence of each mouse in different groups after 21 days of tumor growth.

(F) Photographs of mice tumor luminescence in different groups.

(G) H&E staining of tumor tissue sections after treatment with normal saline or SH-CaO<sub>2</sub> NPs.

Data are represented as mean ± SD; statistical analysis was performed by Student's t test (\*\*\*\*p < 0.0001 versus control).

*in vivo* given that histological analysis and blood physiological-biochemical analysis revealed no pathological changes in the 30 days following injection (Figures S12 and S13), and the maximum tolerated dose of NPs was then determined to be 110 mg/kg (Table S1; Figures S14–S16). Next, the biodistribution of  $\text{Ca}^{2+}$  content in major organs suggested the high aggregation and retention ability of SH- $\text{CaO}_2$  NPs in tumor region, ensuring its excellent tumor-killing effect (Figure S17). In subcutaneously implanted tumor models, there was remarkable antitumor efficacy for SH- $\text{CaO}_2$  NPs, such that the tumor almost disappeared during the 14-day observation period after the intratumor injection (Figures S18 and S19). H&E staining and TUNEL (TdT-mediated dUTP nick-end labeling) immunofluorescence also proved cell death 2 days after the injection (Figure S18C). For orthotopic mouse models, in contrast with the control group that have obvious tumor metastasis, both the injection groups exhibited a significant tumor-growth-inhibition effect without distant metastasis (Figures 6D and 6F). The unchanged body weight during the treatments also suggested the great biocompatibility at a given injection dose (Figure S20). Additionally, H&E staining of tumor sections further illustrated the mass death of tumor cells, compared with the controls, while the histological analysis revealed no damages to major organs (Figures 6G and S21). Overall, these therapeutic studies *in vivo* demonstrated that SH- $\text{CaO}_2$  NPs would be a good candidate for effective anticancer therapy with little potential biological side effects.

## DISCUSSION

We have reported the room-temperature synthesis of pH-sensitive SH- $\text{CaO}_2$  NPs through a rapid wet-chemistry method and examined the ability of these nanoparticles to release free  $\text{Ca}^{2+}$  and  $\text{H}_2\text{O}_2$  in an acidic tumor microenvironment. Because CAT is downregulated in tumor cells, the cells are more vulnerable and easily driven into oxidative stress by excessive cellular  $\text{H}_2\text{O}_2$ , which may alter the calcium channels and result in abnormal retention of the generated  $\text{Ca}^{2+}$  in cells. This kind of calcium overload would irreversibly switch the calcium signals from “regulating” to “destroying” and subsequently induce cell death. Since  $\text{Ca}^{2+}$  are essential in various types of cells, tumor type and oxygen partial pressure do not limit the killing effect. Moreover, SH- $\text{CaO}_2$  NPs are observed to be capable of initiating cell calcification during the therapeutic process, which could further benefit tumor inhibition. Further studies on the specific cell-death pathway of SH- $\text{CaO}_2$  NPs and the mechanism of cell calcification are currently underway. This microenvironment-activated calcification is expected to benefit CT imaging in monitoring the efficacy of treatment.

On a separate note, this calcium-mediated strategy highlights the importance of the biological effects of those metal ions that are often overlooked in conventional tumor treatment, and we summarize this kind of antitumor strategy as “ion-interference therapy.” The *in-situ*-degraded products of nanomaterials—including metal ions, anions, small molecules, and clusters—can really make a difference for tumor treatment with their unique biological effects and interactions with the tumor microenvironment.<sup>33–36</sup> The emergence of ferroptosis and gas therapy (e.g., NO and  $\text{H}_2\text{S}$ ) provides some good examples.<sup>37</sup> With the in-depth understanding of their invisible effects to tumor regions and in turn taking advantage of them, the idea of “ion-interference therapy” will potentially open up a new opportunity for the development of antitumor strategies.<sup>38</sup>

## EXPERIMENTAL PROCEDURES

Full experimental procedures are provided in the [Supplemental Information](#).

## SUPPLEMENTAL INFORMATION

Supplemental Information can be found online at <https://doi.org/10.1016/j.chempr.2019.06.003>.

## ACKNOWLEDGMENTS

The authors greatly acknowledge the financial support from the National Funds for Distinguished Young Scientists (grant 51725202), the National Natural Science Foundation of China (grant 51872094), the National Science Foundation for the Young Scientists of China (grant 51702211), and the Collaborative Innovation Center of Technology and Equipment for Biological Diagnosis and Therapy in Universities of Shandong. We thank Hua Zhang and Shiman Wu (Department of Radiology, Hua-shan Hospital, Fudan University) for the CT imaging and helpful discussion. We thank Dr. Xingwu Jiang and Yelin Wu (Shanghai Tenth People's Hospital, Tongji University School of Medicine) for the establishment of orthotopic tumor models for *in vivo* evaluation. We also thank Chenxi Zhu (Shanghai Institute of Ceramics, Chinese Academy of Sciences) for help on the TEM analysis of nanoparticles.

## AUTHOR CONTRIBUTIONS

Conceptualization, M.Z.; Methodology, M.Z., X.L., and W.B.; Investigation, M.Z., R.S., X.M., Yang Liu, Z.Y., and J.Z.; Writing – Original Draft, M.Z.; Writing – Review & Editing, M.Z., Yanyan Liu, Z.T., Z.Y., X.L., and W.B.; Supervision, X.L. and W.B.; Funding Acquisition, W.B.

## DECLARATION OF INTERESTS

The authors declare no competing interests.

Received: February 21, 2019

Revised: May 15, 2019

Accepted: June 6, 2019

Published: July 3, 2019

## REFERENCES AND NOTES

1. Flament-Durand, J., Ketelbant-Balasse, P., Maurus, R., Regnier, R., and Spehl, M. (1975). Intracerebral calcifications appearing during the course of acute lymphocytic leukemia treated with methotrexate and X rays. *Cancer* 35, 319–325.
2. Drago, P.C., Badalament, R.A., Lucas, J., and Drago, J.R. (1989). Bladder wall calcification after intravesical mitomycin C treatment of superficial bladder cancer. *J. Urol.* 142, 1071–1072.
3. Sheline, G.E., Wara, W.M., and Smith, V. (1980). Therapeutic irradiation and brain injury. *Int. J. Radiat. Oncol. Biol. Phys.* 6, 1215–1228.
4. Keizer, H.G., Pinedo, H.M., Schuurhuis, G.J., and Joenje, H. (1990). Doxorubicin (adriamycin): a critical review of free radical-dependent mechanisms of cytotoxicity. *Pharmacol. Ther.* 47, 219–231.
5. Her, S., Jaffray, D.A., and Allen, C. (2017). Gold nanoparticles for applications in cancer radiotherapy: mechanisms and recent advancements. *Adv. Drug Deliv. Rev.* 109, 84–101.
6. Riley, P.A. (1994). Free radicals in biology: oxidative stress and the effects of ionizing radiation. *Int. J. Radiat. Biol.* 65, 27–33.
7. Cross, B.M., Breitwieser, G.E., Reinhardt, T.A., and Rao, R. (2014). Cellular calcium dynamics in lactation and breast cancer: from physiology to pathology. *Am. J. Physiol. Cell Physiol.* 306, C515–C526.
8. Fleckenstein-grün, G., and Fleckenstein, A. (2009). Calcium — a neglected key factor in arteriosclerosis. The pathogenetic role of arterial calcium overload and its prevention by calcium antagonists. *Ann. Med.* 23, 589–599.
9. Floersheim, G.L. (1992). Calcium antagonists protect mice against lethal doses of ionizing radiation. *Br. J. Rad* 65, 1025–1029.
10. Orrenius, S., Zhivotovsky, B., and Nicotera, P. (2003). Regulation of cell death: the calcium-apoptosis link. *Nat. Rev. Mol. Cell Biol.* 4, 552–565.
11. Liu, L.H., Zhang, Y.H., Qiu, W.X., Zhang, L., Gao, F., Li, B., Xu, L., Fan, J.X., Li, Z.H., and Zhang, X.Z. (2017). Dual-stage light amplified photodynamic therapy against hypoxic tumor based on an O<sub>2</sub> self-sufficient nanoplatform. *Small* 13, 1701621.
12. Huang, C.-C., Chia, W.-T., Chung, M.-F., Lin, K.-J., Hsiao, C.-W., Jin, C., Lim, W.-H., Chen, C.-C., and Sung, H.-W. (2016). An implantable depot that can generate oxygen in situ for overcoming hypoxia-induced resistance to anticancer drugs in chemotherapy. *J. Am. Chem. Soc.* 138, 5222–5225.
13. Doskey, C.M., Buranasudja, V., Wagner, B.A., Wilkes, J.G., Du, J., Cullen, J.J., and Buettner, G.R. (2016). Tumor cells have decreased ability to metabolize H<sub>2</sub>O<sub>2</sub>: implications for pharmacological ascorbate in cancer therapy. *Redox Biol.* 10, 274–284.
14. Ermak, G., and Davies, K.J. (2002). Calcium and oxidative stress: from cell signaling to cell death. *Mol. Immunol* 38, 713–721.
15. Pinton, P., Giorgi, C., Siviero, R., Zecchini, E., and Rizzuto, R. (2008). Calcium and apoptosis: ER-mitochondria Ca<sup>2+</sup> transfer in the control of apoptosis. *Oncogene* 27, 6407–6418.
16. Wang, J., Liu, J., Liu, Y., Wang, L., Cao, M., Ji, Y., Wu, X., Xu, Y., Bai, B., Miao, Q., et al. (2016). Gd-hybridized plasmonic Au-nanocomposites

- enhanced tumor-interior drug permeability in multimodal imaging-guided therapy. *Adv. Mater.* **28**, 8950–8958.
17. Goh, E.J., Kim, K.S., Kim, Y.R., Jung, H.S., Beack, S., Kong, W.H., Scarcelli, G., Yun, S.H., and Hahn, S.K. (2012). Bioimaging of hyaluronic acid derivatives using nanosized carbon dots. *Biomacromolecules* **13**, 2554–2561.
  18. Sperling, R.A., and Parak, W.J. (2010). Surface modification, functionalization and bioconjugation of colloidal inorganic nanoparticles. *Proc. R. Soc. A* **368**, 1333–1383.
  19. Tu, Y. (2016). Artemisinin—a gift from traditional Chinese medicine to the world (Nobel lecture). *Angew. Chem. Int. Ed.* **55**, 10210–10226.
  20. Yan, Y., Wei, C.L., Zhang, W.R., Cheng, H.P., and Liu, J. (2006). Cross-talk between calcium and reactive oxygen species signaling. *Acta Pharmacol. Sin.* **27**, 821–826.
  21. Kiselyov, K., and Muallem, S. (2016). ROS and intracellular ion channels. *Cell Calcium* **60**, 108–114.
  22. Görlach, A., Bertram, K., Hudecova, S., and Krizanova, O. (2015). Calcium and ROS: a mutual interplay. *Redox Biol.* **6**, 260–271.
  23. Brookes, P.S., Yoon, Y., Robotham, J.L., Anders, M.W., and Sheu, S.-S. (2004). Calcium, ATP, and ROS: a mitochondrial love-hate triangle. *Am. J. Physiol. Cell Physiol* **287**, C817–C833.
  24. Votyakova, T.V., and Reynolds, I.J. (2005). Ca<sup>2+</sup>-induced permeabilization promotes free radical release from rat brain mitochondria with partially inhibited complex I. *J. Neurochem.* **93**, 526–537.
  25. Cheng, H., and Lederer, W.J. (2008). Calcium sparks. *Physiol. Rev.* **88**, 1491–1545.
  26. Cheng, H., Lederer, M.R., Lederer, W.J., and Cannell, M.B. (1996). Calcium sparks and [Ca<sup>2+</sup>]<sub>i</sub> waves in cardiac myocytes. *Am. J. Physiol. Cell Physiol.* **270**, C148–C159.
  27. Duchen, M.R. (2000). Mitochondria and calcium: from cell signalling to cell death. *J. Physiol.* **529**, 57–68.
  28. Zhang, C., Ni, D., Liu, Y., Yao, H., Bu, W., and Shi, J. (2017). Magnesium silicide nanoparticles as a deoxygenation agent for cancer starvation therapy. *Nat. Nanotechnol.* **12**, 378–386.
  29. Anderson, H.C. (2003). Matrix vesicles and calcification. *Curr. Rheumatol. Rep.* **5**, 222–226.
  30. Anderson, H.C. (1995). Molecular biology of matrix vesicles. *Clin. Orthop. Relat. Res.* **266**–280.
  31. Zhao, R., Wang, B., Yang, X., Xiao, Y., Wang, X., Shao, C., and Tang, R. (2016). A drug-free tumor therapy strategy: cancer-cell-targeting calcification. *Angew. Chem. Int. Ed.* **55**, 5225–5229.
  32. Kim, S., Palanikumar, L., Choi, H., Jeena, M.T., Kim, C., and Ryu, J.-H. (2018). Intra-mitochondrial biomineralization for inducing apoptosis of cancer cells. *Chem. Sci.* **9**, 2474–2479.
  33. Lin, L.S., Song, J., Song, L., Ke, K., Liu, Y., Zhou, Z., Shen, Z., Li, J., Yang, Z., Tang, W., et al. (2018). Simultaneous Fenton-like ion delivery and glutathione depletion by MnO<sub>2</sub>-based nanoagent to enhance chemodynamic therapy. *Angew. Chem. Int. Ed.* **130**, 4996–5000.
  34. Zhou, W., Pan, T., Cui, H., Zhao, Z., Chu, P.K., and Yu, X.F. (2019). Black phosphorus: bioactive nanomaterials with inherent and selective chemotherapeutic effects. *Angew. Chem. Int. Ed.* **131**, 779–784.
  35. Zhang, Y., Yang, Y., Jiang, S., Li, F., Lin, J., Wang, T., and Huang, P. (2018). Degradable silver-based nanoplatfor for synergistic cancer starving-like/metal ion therapy. *Mater. Horiz.* **6**, 169–175.
  36. Li, X., Wang, X., Zhang, J., Hanagata, N., Wang, X., Weng, Q., Ito, A., Bando, Y., and Golberg, D. (2017). Hollow boron nitride nanospheres as boron reservoir for prostate cancer treatment. *Nat. Commun.* **8**, 13936.
  37. Stockwell, B.R., Friedmann Angeli, J.P.F., Bayir, H., Bush, A.I., Conrad, M., Dixon, S.J., Fulda, S., Gascón, S., Hatzios, S.K., Kagan, V.E., et al. (2017). Ferroptosis: a regulated cell death nexus linking metabolism, redox biology, and disease. *Cell* **171**, 273–285.
  38. Zhang, M., Shen, B., Song, R., Wang, H., Bin, L., Meng, X., Liu, Y., Liu, Y., Zheng, X., Su, W., et al. (2019). Radiation-assisted metal ion interference tumor therapy by barium peroxide-based nanoparticles. *Mater. Horiz.* **6**, 1034–1040.